J Neurophysiol 94: 1688–1698, 2005.
First published May 25, 2005; 10.1152/jn.00284.2005.

Comparison of the Inhibition of Renshaw Cells During Subthreshold and Suprathreshold Conditions Using Anatomically and Physiologically Realistic Models

Tuan V. Bui,[1] Dianne E. Dewey,[2] Robert E. W. Fyffe,[2] and P. Ken Rose[1]

[1]*Canadian Institute for Health Research Group in Sensory-Motor Systems, Department of Physiology, Centre for Neuroscience Studies, Queen's University, Kingston, Canada; and* [2]*Department of Anatomy, Wright State University, Dayton, Ohio*

Submitted 16 March 2005; accepted in final form 18 May 2005

Bui, Tuan V., Diane E. Dewey, Robert E. W. Fyffe, and P. Ken Rose. Comparison of the inhibition of Renshaw cells during subthreshold and suprathreshold conditions using anatomically and physiologically realistic models. *J Neurophysiol* 94: 1688–1698, 2005. First published May 25, 2005; 10.1152/jn.00284.2005. Inhibitory synaptic inputs to Renshaw cells are concentrated on the soma and the juxtasomatic dendrites. In the present study, we investigated whether this proximal bias leads to more effective inhibition under different neuronal operating conditions. Using compartmental models based on detailed anatomical measurements of intracellularly stained Renshaw cells, we compared the inhibition produced by glycine/γ-aminobutyric acid-A ($GABA_A$) synapses when distributed with a proximal bias to the inhibition produced when the same synapses were distributed uniformly (i.e., with no regional bias). The comparison was conducted in subthreshold and suprathreshold conditions. The latter were mimicked by voltage clamping the soma to −55 mV. The voltage clamp reduces nonlinear interactions between excitatory and inhibitory synapses. We hypothesized that for electrotonically compact cells such as Renshaw cells, the strength of the inhibition would become much less dependent on synaptic location in suprathreshold conditions. This hypothesis was not confirmed. The inhibition produced when inhibitory inputs were proximally distributed was always stronger than when the same inputs were uniformly distributed. In fact, the relative effectiveness of proximally distributed inhibitory inputs over uniformly distributed synapses was greater in suprathreshold conditions than that in subthreshold conditions. The somatic voltage clamp minimized saturation of inhibitory driving potentials. Because this effect was greatest near the soma, the current produced by more distal synapses suffered a greater loss because of saturation. Conversely, in subthreshold conditions, the effectiveness of proximal synapses was substantially reduced at high levels of background synaptic activity because of saturation. Our results suggest glycine/$GABA_A$ synapses on Renshaw cells are strategically distributed to block the powerful excitatory drive produced by recurrent collaterals from motoneurons.

INTRODUCTION

Renshaw cells are a unique class of spinal interneurons. They send inhibitory projections to motoneurons and, in turn, they are the primary target of axon collaterals of motoneurons (Eccles et al. 1954; Renshaw 1946). These collaterals form a powerful excitatory connection such that in response to motor axon stimulation, Renshaw cells fire a burst of action potentials whose frequency can be >1,000 Hz (Eccles et al. 1956; Hultborn and Pierrot-Deseilligny 1979; Ryall 1970; Walmsley and Tracey 1981). This connection is sufficiently strong that stimulation of a single motor axon can elicit a disynaptic inhibitory postsynaptic potential (IPSP) in motoneurons of the same motor pool (Hamm et al. 1987; Ross et al. 1976; Van Keulen 1981). The strength of this connection can also be measured in anatomical terms: assuming a uniform density of five synapses for every 100 μm^2 of membrane surface area for Renshaw cells (Lagerback 1983), the cholinergic synapses formed by the axon collaterals of motoneurons represent the majority of all excitatory synapses on the dendritic trees of Renshaw cells (Alvarez et al. 1999).

Inhibitory synapses to Renshaw cells, originating from other Renshaw cells (Ryall 1970) or descending inputs (Baldiserra et al. 1981; Katz and Pierrot-Deseilligny 1999), seem to be ideally positioned to counteract the powerful excitatory connections originating from motoneurons. Immunostaining for the glycine receptor clustering protein, gephyrin, and for γ-aminobutyric acid-A ($GABA_A$) receptors shows large clusters of glycine/$GABA_A$ receptors that are mainly located on the soma and juxtasomatic regions of the dendritic tree (Alvarez et al. 1997; Geiman et al. 2002). It has been estimated that these glycinergic/GABAergic synapses account for 75–80% of all synapses on the soma and most proximal dendrites of Renshaw cells (Alvarez et al. 1999). As indicated by Koch et al. (1983), inhibition is most effective if it is positioned on the path between an excitatory synapse and the soma. For large excitatory conductances, Koch et al. (1983) demonstrated that the optimal location for the inhibition moves toward the soma while staying on the path of the excitation. Thus the distribution of the glycinergic/GABAergic synapses to Renshaw cells precisely fulfills the criterion for maximal inhibition. There are two caveats to such a conclusion, however. First the conclusion that proximally distributed inhibition is more effective was derived analytically assuming that the cell was operating in subthreshold conditions, that is, when the membrane potential is below the threshold for firing action potentials (Koch 1999). Second, the electrotonic structure of Renshaw cells is compact (Bui et al. 2003). Thus inputs to Renshaw cells do not generally suffer from great attenuation and there may not be significant differences in the inhibition produced by proximally and distally distributed inhibitory inputs.

In subthreshold conditions, the activity of excitatory and inhibitory synapses can mutually change their respective driving potential. These interactions can lead to sublinear arith-

Address for reprint requests and other correspondence: T. Bui, Department of Physiology, Botterell Hall, Queen's University, Kingston K7L 3N6, Canada (E-mail: tuan@biomed.queensu.ca).

The costs of publication of this article were defrayed in part by the payment of page charges. The article must therefore be hereby marked "*advertisement*" in accordance with 18 U.S.C. Section 1734 solely to indicate this fact.

metic, in which inhibition acts divisively rather than subtractively (Rall 1977; Ulrich 2003). However, the repetitive firing of action potentials in suprathreshold conditions introduces a virtual clamping of the membrane potential that adds a different element to the integration of synaptic inputs (Holt and Koch 1997; Koch 1999). In this situation, the driving potentials of both excitatory and inhibitory synapses can be constant, leading to linear rather than nonlinear interactions. Because the origin of the voltage clamp introduced by repetitive firing is somatic, it is not surprising that proximal inhibition has been observed to be subtractive in suprathreshold conditions (Brizzi et al. 2004; Gabbiani et al. 1994; Holt and Koch 1997; Ulrich 2003). However, considering the potentially limited spatial extent of the voltage clamp, it is surprising that distal inhibition has been observed to be subtractive as well (Holt and Koch 1997). In such cases where the inhibitory effects of synapses located both proximally and distally are purely subtractive, the differences in effectiveness between proximal and distal inhibition may solely be a function of the currents that they can deliver to the cell body. In electrotonically compact cells such as Renshaw cells, the differences in currents delivered by proximally and distally distributed inputs are negligible at low levels of synaptic activity (Bui et al. 2003), assuming that the number of synapses is the same for both distributions. Therefore the strategic advantage of proximal inhibition may be reduced in the suprathreshold regime compared with the subthreshold regime for Renshaw cells. Our goal was to verify this prediction.

To meet this objective, we constructed compartmental models based on detailed anatomical measurements of the dendritic geometry of four intracellular stained Renshaw cells. In one set of models, the cholinergic and glycinergic/GABAergic synapses were arranged according to their known distribution pattern (Alvarez et al. 1997, 1999). In a second set of models, the glycinergic/GABAergic synapses were redistributed more distally such that their density (number/100 μm^2) was the same on the entire somatic and dendritic surface. Various levels of synaptic activity were simulated in current-clamp mode to replicate subthreshold conditions and with a somatic voltage clamp to replicate suprathreshold conditions. We then compared the inhibition produced by the two distributions of inhibitory inputs on the somatic membrane potential changes produced by excitatory synaptic activity in subthreshold conditions, and the currents arriving at the cell body produced by excitatory synaptic activity in suprathreshold conditions. Unexpectedly, our results contradict our hypothesis that the strategic advantages of proximal inhibition are lost in the suprathreshold regime.

METHODS

Compartmental modeling

The construction of the compartmental models of Renshaw cells was described in detail in Bui et al. (2003). The value of the specific resistivity of the cytoplasm (R_i) selected for this study, 70 $\Omega \cdot$ cm, is based on calculations for motoneurons (Barrett and Crill 1974) and is close to the value for saline (Hille 2001). In subthreshold conditions, the value of the specific resistivity of the membrane (R_m) was 15,000 $\Omega \cdot cm^2$ for all four cells. In suprathreshold conditions, R_m was modified to reflect the change in input conductance caused by the synaptic activity required to bring the membrane potential up to −55 mV, the assumed average membrane potential during repetitive firing of action potentials. Thus for simulations of suprathreshold conditions, R_m values were in the range of 13,500–14,000 $\Omega \cdot cm^2$ for the four cells.

Simulations were performed using Saber, a mixed-signal simulator software package (Synopsys, Mountain View, CA) (Carnevale et al. 1990). To calculate the total synaptic current that reaches the soma, the membrane potential of the cell body was clamped to −55 mV for simulations of suprathreshold conditions. This is analogous to the experimental technique developed by Heckman and Binder (1988)

Synaptic innervation

The distribution of excitatory synapses was based on the arrangement of cholinergic synapses on Renshaw cells as described by Alvarez et al. (1999). For the soma and the proximal 50 μm, excitatory synapses were distributed at a density of one synapse per 100 μm^2. For all other regions of the dendritic tree, excitatory synapses were distributed at a density of four synapses per 100 μm^2.

The density of glycine/GABAergic inputs to Renshaw cells were inferred from observations by Alvarez et al. (1997, 1999). According to Alvarez et al. (1999), F-type synapses (glycinergic synapses) constitute 75–80% of all synapses on the soma, whereas S-type synapses constitute 10% of all somatic synapses and 20% of proximal synapses. If we assume that the density of cholinergic synapses (one synapse per 100 μm^2) represents 10% of all somatic synapses, then according to the above estimates, the somatic density of glycine/GABAergic inputs is eight synapses per 100 μm^2. To calculate the density of glycine/GABAergic synapses on the dendrites, we extrapolated the relative density of these inputs to the somatic, proximal, and distal dendritic regions of Renshaw cells using Table 1 of Alvarez et al. (1997) where they report the means of gephyrin-immunoreactive clusters measured in different distance bins. The number of clusters sampled differed in different regions, usually reflecting the dendritic surface area. Using our own morphological analysis of reconstructed Renshaw cells (Bui et al. 2003), we calculated the cumulative membrane surface area that was found in each distance bin. Dividing the number of clusters by the cumulative membrane surface area found within the matching distance bin provides a relative density of glycinergic/GABAergic synapses. The results of this analysis are found in Table 1 and were used to set the density of glycine/GABA inputs in the dendritic regions closer than 100 μm from the soma at eight synapses/100 μm^2, and those $\geq$100 μm away from the soma to be two synapses/100 μm^2. The latter density may be an overestimate for dendritic regions >200 μm from the soma. However, the number of clusters found between 100 and 200 μm away from the soma and >200 μm from the soma is small. Their relative difference may therefore be exaggerated. For this reason, we assigned the same densities of clusters to both regions.

In a second set of models, the inhibitory synapses were distributed uniformly on the same four model cells. The number of synapses for each cell was kept constant to assess the effects of distribution solely.

TABLE 1. *Estimation of relative glycine/GABA inputs to Renshaw cells*

	Distance, μm		
	0–100	100–200	200–500
Number of clusters	148	39	23
Total surface area, μm^2	13,789	15,129	32,680
Density of clusters, cluster/100 μm^2	1.07	0.26	0.07
Relative density of clusters	15.2	3.7	1

Data on number of clusters and total surface area were taken from Table 1 of Alvarez et al. (1997). Data on density of clusters were taken from four reconstructions of cat Renshaw cells (Bui et al. 2003).

Thus for the four models, the densities (number of synapses in parentheses) of glycine/GABA synapses when distributed uniformly throughout the dendritic tree were 3.6 synapses/100 μm^2 (604), 3.3 synapses/100 μm^2 (1,026), 3.8 synapses/100 μm^2 (441), and 4.8 synapses/100 μm^2 (499).

Modeling synaptic conductance changes

Current injected by synaptic activation (i_{syn}) is a product of the conductance generated by channel opening and the driving potential, such that

$$i_{syn} = g(E_{rev} - V_m) \quad (1)$$

where g is the synaptic conductance change, E_{rev} is the reversal potential, and V_m is the membrane potential. The parameters describing the conductance change of the glycinergic/GABAergic and the cholinergic synapses to Renshaw cells were estimated using data gathered in different studies.

Cholinergic inputs to Renshaw cells

The subunit composition of the cholinergic receptors of Renshaw cells is $\alpha_4\beta_2$ (Dourado and Sargent 2002), indicating that cholinergic transmission to Renshaw cells is mediated by nicotinic receptors. The 10–90% rise time was estimated to be 1.0 ms at 23°C. If we assume Q10 to be 3 and a temperature of 37°C, a scaling factor of $3^{1.4} = 4.7$ is used to adjust the time-course measurements of Dourado and Sargent (2002). Thus the 10–90% rise time was reduced to 0.21 ms. Assuming that the time course of the conductance change can be modeled as an α-function, a 10–90% rise time of 0.21 ms corresponds to a time to peak (t_{peak}) of 0.36 ms. The decay time constant (τ_1) measured by Dourado and Sargent (2002) was 5 ms (1.1 ms at 37°C). Because an alpha function with a t_{peak} of 0.36 ms has a shorter decay time constant, we used a piecewise function that is described by an alpha function with a time to peak of 0.36 ms (and a 10–90% rise time of 0.21 ms) for the rising phase and an exponential decay with a decay time constant (τ_1) of 1.1 ms for the decay phase. Thus the conductance change for cholinergic synapses to Renshaw cells, $g_{nACh}(t)$, is given as

$$g_{nACh}(t) = \begin{cases} \dfrac{g_{peak} e t e^{-t/t_{peak}}}{t_{peak}} & t < t_{peak} \\ g_{peak} e^{-(t - t_{peak})/\tau_1} & t > t_{peak} \end{cases} \quad (2)$$

The tonic conductance change of such a conductance time course is given by the time-averaged conductance change (Bernander et al. 1991), in this case

$$\begin{aligned} \bar{g}_{nACh} &= \int g_{nACh}(t) \\ &= \int_0^{t_{peak}} \frac{g_{peak} e t e^{-t/t_{peak}}}{t_{peak}} dt + \int_{t_{peak}}^{\infty} g_{peak} e^{-(t - t_{peak})/\tau_1} dt \\ &= g_{peak} e t_{peak} \left(\frac{-2}{e} + 1 \right) + g_{peak}(\tau_1) \end{aligned} \quad (3)$$

The selected value of the peak unitary nicotinic conductance, g_{peak}, was based on unitary nicotinic conductances obtained from an in vivo study of rat superior cervical ganglion (Sacchi et al. 1998). The mean peak conductance was estimated to be 4.0 nS. However, the nicotinic receptors of the superior cervical ganglion are composed of the $\alpha_3\beta_4$ (Covernton et al. 1994). Single-channel conductances of the $\alpha_3\beta_4$ receptor (Haghighi and Cooper 1998; Nelson and Lindstrom 1999) are comparable to those of $\alpha_4\beta_2$ receptors (Buisson et al. 1996; Charnet et al. 1992; Figl et al. 1998) and thus we adopted 4.0 nS as the peak unitary amplitude of $\alpha_4\beta_2$ receptors.

The channels associated with the $\alpha_4\beta_2$ receptor exhibit an inward rectification near 0 mV. Thus the reversal potential has to be extrapolated. Reported estimates of reversal potential are based on patch-clamp recordings of expressed $\alpha_4\beta_2$ channels. Haghighi and Cooper (1998) report a reversal potential of −5 mV (unpublished observation) for $\alpha_4\beta_2$ receptors in the rat superior cervical ganglion. This value was used in this study.

Glycinergic/GABAergic inputs to Renshaw cells

Dual-component glycine/GABA inhibitory postsynaptic currents (IPSCs) have been recorded in the spinal cord for several populations of neurons (Jonas et al. 1998; Keller et al. 2001; Schneider and Fyffe 1992). To the best of our knowledge, unitary IPSCs for Renshaw cells have not been reported. Thus our model of the glycine/GABA synapse is based on the recordings of unitary glycine/GABA IPSCs on motoneurons (Jonas et al. 1998).

The time course of unitary glycine/GABA IPSC has a rising phase with a single time constant and a dual-component decay with two time constants, one slow and one fast. Thus a piecewise function was also used to describe the time course of unitary glycine/GABA IPSCs. The rising phase is modeled as the rising phase of an alpha function until t_{peak}. Beyond t_{peak}, the decay phase is modeled as a biexponential decay function with parameters τ_1 and τ_2 corresponding to the fast and slow time constants, respectively. Thus the conductance change for glycine/GABA synapses to Renshaw cells, $g_{gly/GABA}(t)$, is given as

$$g_{gly/GABA}(t) = \begin{cases} \dfrac{g_{peak} e t e^{-t/t_{peak}}}{t_{peak}} & t < t_{peak} \\ g_{peak}(A e^{-(t - t_{peak})/\tau_1} + B e^{-(t - t_{peak})/\tau_2}) & t > t_{peak} \end{cases} \quad (4)$$

where A and B are constants representing the proportion of the two time constants to the total conductance change. As reported by Jonas et al. (1998), A and B are 0.74 and 0.26. The tonic conductance of such a conductance time course is given as

$$\begin{aligned} \bar{g}_{gly/GABA} &= \int g_{gly/GABA}(t) \\ &= \int_0^{t_{peak}} \frac{g_{peak} e t e^{-t/t_{peak}}}{t_{peak}} dt + \int_{t_{peak}}^{\infty} g_{peak}(A e^{-(t - t_{peak})/\tau_1} + B e^{-(t - t_{peak})/\tau_2}) dt \\ &= g_{peak} e t_{peak} \left(\frac{-2}{e} + 1 \right) + g_{peak}(A\tau_1 + B\tau_2) \end{aligned} \quad (5)$$

The values of t_{peak}, τ_1, and τ_2 are taken from Jonas et al. (1998). The value of t_{peak} is extrapolated from the measured 20–80% rise time of 0.46 ms. Because the measurements were taken at 25°C, we applied a scaling factor of $3^{1.2} = 3.7$, assuming again that Q10 is 3. Thus the adjusted 20–80% rise time is 0.13 ms. Assuming that the time course of the conductance change is modeled as an alpha function, the time to peak is estimated to be 0.32 ms. The approximated values of τ_1 and τ_2, adjusted by a scaling factor of 3.7, are respectively 2.7 and 12.2 ms.

The peak conductance of the unitary IPSCs recorded by Jonas et al. (1998) can be estimated by calculating the Cl^- equilibrium potential (E_{Cl^-}) in their whole cell patch-clamp experiments. The internal and external Cl^- concentrations were 144 (or 149) and 133.5 mM, respectively. Using the Nernst equation

$$E_{Cl^-} = -61.5 \ln \left(\frac{144}{133.5} \right) = 4.65 \text{ mV}$$

Subsequently, we can calculate the peak conductance that produced a peak amplitude of 330 pA at −50 mV (Jonas et al. 1998)

$$(-50 \text{ mV} - 4.65 \text{ mV}) = \frac{3.3 \times 10^{-10} \text{A}}{g_{peak}}$$

TABLE 2. *Parameters of cholinergic (nACh) and glycine/GABA synapses onto Renshaw cells*

Parameter	nACh	Glycine/GABA
t_{peak}, ms	0.36	0.32
τ_1, ms	1.1	2.7
τ_2, ms	—	12.2
g_{peak}, nS	4.0	12.2
$\bar{g}$, nS^{-1} ms^{-1}	5.4	65.9
E_{rev}, mV	−5.0	−81.0

$$g_{peak} = 6.1 \text{ nS}$$

Cluster sizes of glycine receptors on motoneurons are on average three times smaller than those on Renshaw cells (Alvarez et al. 1997). Furthermore, there is evidence that cluster size is correlated to the miniature IPSC size in the spinal cord (Oleskevich et al. 1999). To reflect this size-dependent scaling of unitary glycine/GABA unitary conductances, g_{peak} was scaled. Because the developmental scaling of the GABA component with gephyrin cluster size may be smaller than that of the glycinergic component (Gonzàlez-Forero et al. 2005), an arbitrary factor of 2 was used and the peak conductance was increased to 12.2 nS.

Because the glycine/GABA synapse is a chloride-mediated current, a reversal potential value of −81 mV was used as calculated by Stuart and Redman (1990) for glycinergic IPSCs in in vivo motoneurons.

The parameters describing the nicotinic cholinergic synapse and the glycine/GABA synapses on Renshaw cells are detailed in Table 2.

Measures of synaptic activity

To calculate the instantaneous hyperpolarizing current injected by the activation of each additional inhibitory synapse (proximal inhibition: $dI_N/dsynapse_{i,prox}$; uniform inhibition: $dI_N/dsynapse_{i,uni}$) and the instantaneous somatic membrane potential change produced by the activation of each additional inhibitory synapse (proximal inhibition: $d\Delta V_m/dsynapse_{i,prox}$; uniform inhibition: $d\Delta V_m/dsynapse_{i,uni}$), the relations between the current arriving at the cell body (I_N) and the number of inhibitory synapses (x), and the relation between somatic membrane potential change (ΔV_m) and x were respectively fitted by a hyperbolic decay equation (see Fig. 2)

$$I_N(x) = I_N(0) + \frac{ab}{b + x} \quad (7)$$

$$\Delta V_m(x) = V_m(0) + \frac{ab}{b + x} \quad (8)$$

The regressions were performed by SigmaPlot (SPSS, Point Richmond, CA) and the r^2 values were consistently >0.999. Subsequently, the derivative of I_N and of ΔV_m with respect to the number of inhibitory synapses activated were calculated using SigmaPlot to obtain $dI_N/dsynapse_{i,prox}$ and $dI_N/dsynapse_{i,uni}$, and $d\Delta V_m/dsynapse_{i,prox}$ and $d\Delta V_m/dsynapse_{i,uni}$, respectively.

RESULTS

Synaptic distribution

The response to steady-state excitatory and inhibitory synaptic activity was determined for four Renshaw cells. Two different distributions of inhibitory synaptic inputs were modeled (see METHODS). The first distribution, referred to as *proximal inhibition*, was based on anatomical observations of gephyrin clusters in Renshaw cells (Alvarez et al. 1997). For the four Renshaw cells modeled, inhibitory synapses had a median distance from the cell body of 160, 165, 95, and 65 μm, respectively. Subsequently all synapses were redistributed to a more distal distribution; specifically, all inhibitory synapses were redistributed to a uniformly constant density distribution, referred to as *uniform inhibition*. After this redistribution, the median distance from the cell body of inhibitory inputs was 285, 280, 210, and 150 μm, respectively, for the same four cells. The distribution of excitatory synapses was the same in both proximal and uniform inhibition models. Figure 1 shows the distribution of inhibitory synapses, both proximal and uniform, as well as the distribution of excitatory synapses with

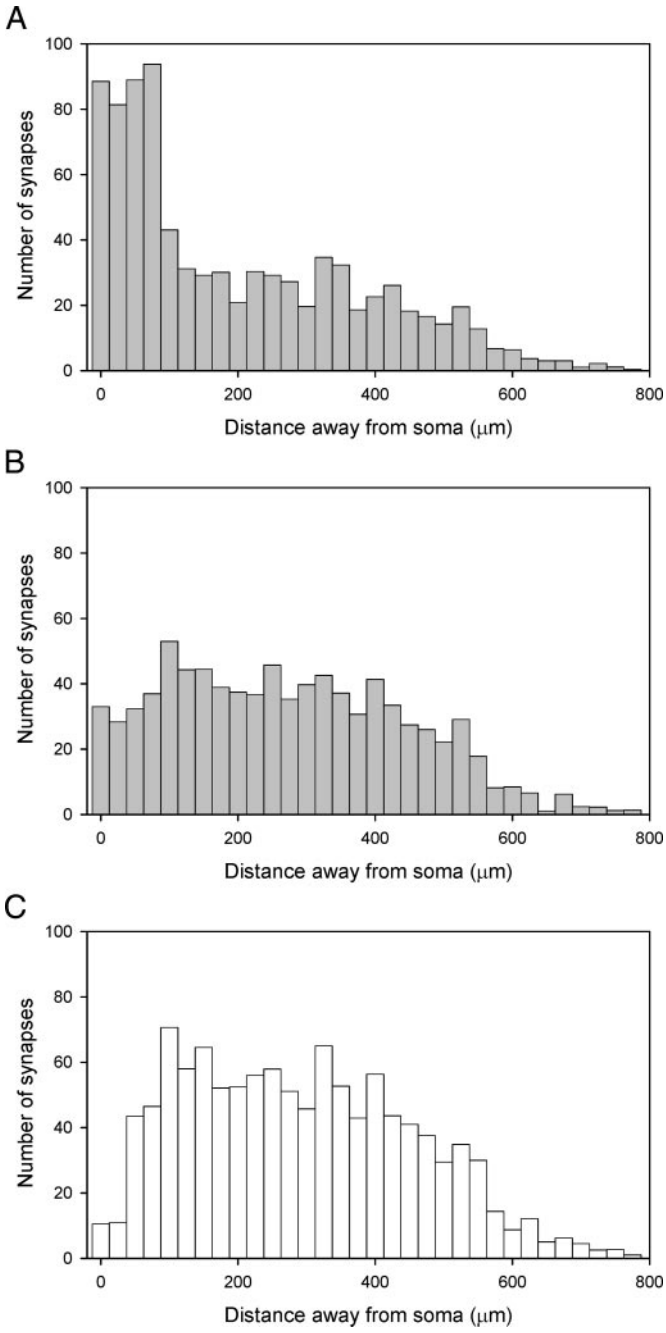

FIG. 1. Histograms of the number of excitatory synapses and inhibitory synapses distributed in a model for one of the Renshaw cells. *A*: inhibitory synapses distributed under proximal inhibition. *B*: inhibitory synapses distributed under uniform inhibition. *C*: excitatory synapses.

relation to distance from the cell body for one of the Renshaw cells (RC2a). The observed decrease in the number of synapses at greater distance away from the soma in the uniform distribution is attributed to the smaller amount of available membrane surface area at greater distance from the cell body (Bui et al. 2003). Note that for graphical simplicity, all subsequent figures (except Fig. 3*B*) illustrate data from this cell. The three other cells showed the same qualitative behavior as that of this cell. For all simulations, the steady-state frequencies of activation of the excitatory synapses and inhibitory synapses were 50 and 10 Hz, respectively.

Suprathreshold regime

A somatic voltage clamp of −55 mV was applied to simulate the average membrane potential of the soma during repetitive firing (suprathreshold state), and the current reaching the cell body (I_N) was measured for different levels of synaptic excitatory and synaptic inhibitory activity (Fig. 2, *A* and *B*). The shape of the relationship between I_N and inhibitory synaptic activity does not vary with the level of excitation. Instead, increasing the level of excitation shifted the relationship upward.

To compare the effectiveness of the inhibition produced by two different distributions under the suprathreshold condition, we calculated the difference in inhibition (ΔI_{inh}), which is simply the difference in I_N with proximal inhibition and that with uniform inhibition. This measure represents the increase in inhibition produced when the synapses are distributed proximally rather than uniformly. As can be seen in Fig. 2*C*, proximal inhibition is more potent than uniform inhibition. This difference increases with the level of inhibitory activity. However, ΔI_{inh} is largely independent of the level of excitatory activity.

Subthreshold regime

In the subthreshold regime, the membrane potential of the soma is not clamped by the repetitive firing of action potentials (Koch et al. 1995). The effectiveness of the two distributions of inhibitory inputs was compared under current-clamp conditions and the changes in membrane potential at the soma (ΔV_m) were measured (resting membrane potential = −64 mV). Because we previously defined threshold as −55 mV, simulation results where the somatic membrane potential was below −55 mV ($\Delta V_m < -9$ mV) are shown in black to highlight the subthreshold regime (Fig. 2, *D* and *E*). Unlike the suprathreshold regime, the shape of the relation between ΔV_m and inhibitory synaptic activity changes with the level of excitation.

The difference in inhibition (ΔV_{inh}) under subthreshold conditions was calculated as the difference in ΔV_m produced during the two types of inhibition (Fig. 2*F*). As was observed in the suprathreshold state, the inhibition produced by proximal inhibition was stronger than that produced by uniform inhibition at all levels of excitatory and inhibitory synaptic activity. However, ΔV_{inh} increases with increasing levels of excitatory activity and is relatively insensitive to the level of inhibitory activity.

Comparison of proximal and uniform inhibition in subthreshold and suprathreshold conditions

Although ΔI_{inh} is the appropriate measure to compare the effectiveness of proximal versus uniform inhibition under suprathreshold conditions and ΔV_{inh} is the appropriate measure to compare the effectiveness of proximal versus uniform inhibition under subthreshold conditions, it is difficult to compare ΔI_{inh} to ΔV_{inh} because these measures relate to two different electrical measures. To address this problem, we compared the inhibition produced by proximally and uniformly distributed synapses by determining the level of synaptic activity of uniform inhibition required to match the inhibition produced by a particular level of proximal inhibition (Fig. 3). This comparison, made at various levels of background excitatory synaptic activity, is shown for the suprathreshold regime in Fig. 3*A* (*left*) and the subthreshold regime in Fig. 3*A* (*right*). Points above the line of unity indicate that for that particular level of proximal inhibition, a higher level of uniform inhibition is required to produce the equivalent inhibition. Because proximal inhibition was always more effective than uniform inhibition, it is not surprising that all points are above the line of unity. To determine whether proximal inhibition was even more effective than uniform inhibition in suprathreshold conditions as opposed to subthreshold conditions, we calculated the percentage increase in level of uniform inhibition required to match a corresponding level of proximal inhibition. The results for all four Renshaw cells are presented in Fig. 3*B*. Points below 0 indicate that when the cell moved from the subthreshold regime to the suprathreshold regime, a decrease in the level of uniform inhibition was required to match a particular level of proximal inhibition. In such cases, proximal inhibition was more effective than uniform inhibition, although this difference was reduced when the cell moved from subthreshold regime to the suprathreshold regime. Conversely, points above 0 indicate that when the cell moved from the subthreshold regime to the suprathreshold regime, an increase in the level of uniform inhibition was required to match a particular level of proximal inhibition. Thus for almost all levels of synaptic excitation, proximal inhibition was even more effective than uniform inhibition in suprathreshold conditions, although these differences became less pronounced at higher levels of excitation. This contradicts our prediction that in the suprathreshold regime the differences between proximal and more distal inhibition would become negligible for Renshaw cells.

Mechanisms that enhance the effectiveness of proximal versus uniform inhibition in the suprathreshold regime

To determine the mechanisms that increased the effectiveness of proximal inhibition versus suprathreshold conditions, we examined the instantaneous output of inhibitory synapses to Renshaw cells at different levels of synaptic activity. As synaptic activity increases, changes in driving potential lead to changes in synaptic output. Thus the inhibition contributed by additional inhibitory synapse decreases with increasing inhibitory activity but increases with increasing excitatory activity. These changes reflect the reduction of the inhibitory driving potential produced by each activated inhibitory synapse and, conversely, the increase of the inhibitory driving potential

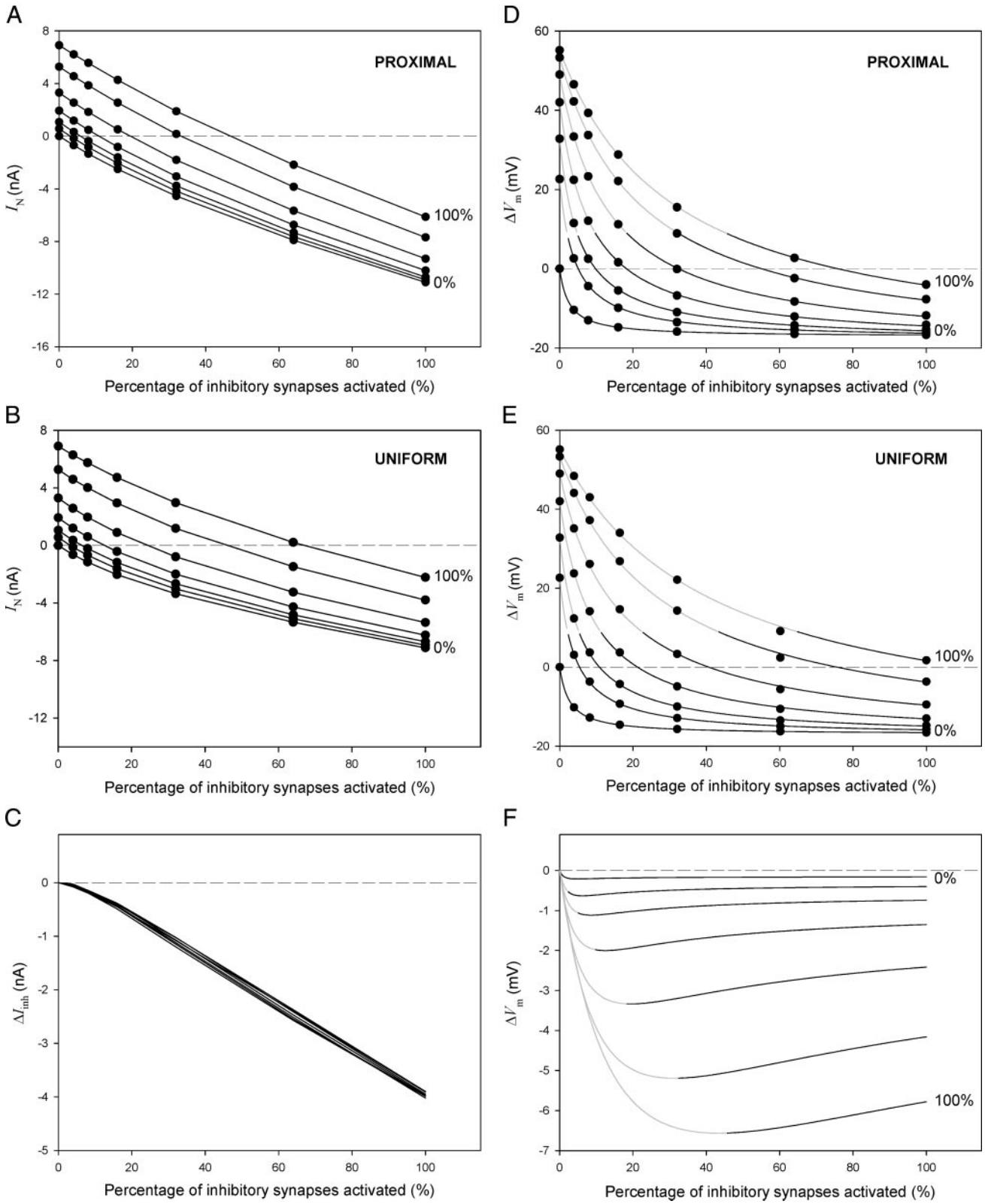

FIG. 2. Current arriving at the cell body (I_N) at varying levels of excitatory and inhibitory activity during suprathreshold conditions; and somatic membrane potential change (ΔV_m) at varying levels of excitatory and inhibitory activity during subthreshold conditions. Numbers at the *right* of each curve (all except for *C*) indicate the level of excitatory activity. From *top to bottom* (except for *F*), curves represent measurements with 100, 64, 32, 16, 8, 4, and 0% activation of total excitatory synapses. Filled circles represent measurements; lines represent fits as described in METHODS. Gray lines represent conditions under which the somatic membrane potential would exceed the threshold for repetitive activity in subthreshold conditions. *A*: I_N with proximal inhibition. *B*: I_N with uniform inhibition. *C*: difference in somatic inhibitory current (ΔI_{inh}) under suprathreshold conditions. Curves represent measurements with 100, 64, 32, 16, 8, 4, and 0% activation of total excitatory synapses. Curves are not marked for graphical clarity. *D*: ΔV_m with proximal inhibition. *E*: ΔV_m with uniform inhibition. *F*: difference in inhibitory somatic membrane potential change (ΔV_{inh}) under subthreshold conditions. From *top to bottom*, curves represent measurements with 0, 4, 8, 16, 32, 64, and 100% activation of total excitatory synapses.

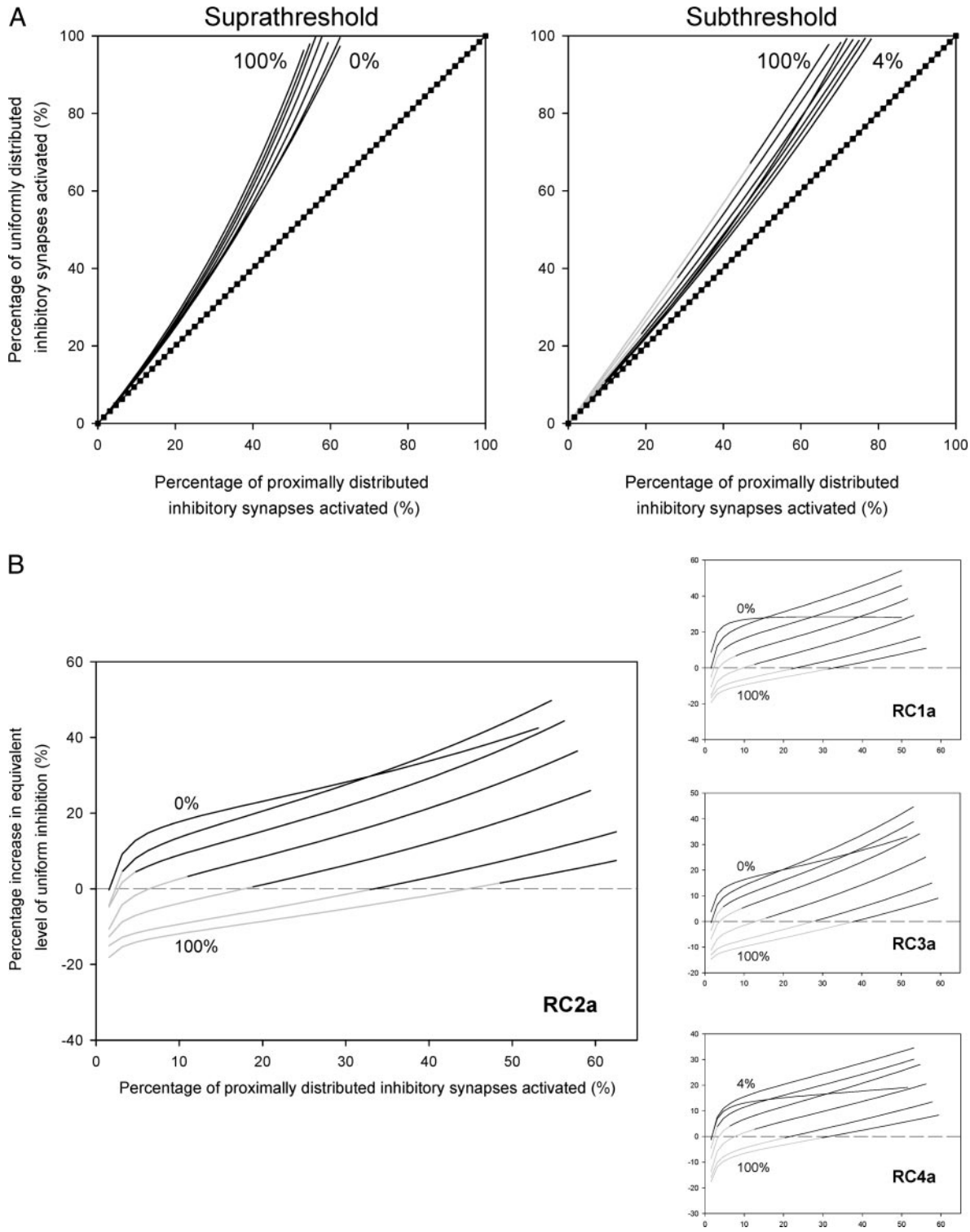

FIG. 3. *A*: equivalent levels of uniform inhibition and proximal inhibition under suprathreshold (*left*) and subthreshold (*right*) conditions. In suprathreshold conditions, from *left to right*, curves represent measurements with 100, 64, 32, 16, 8, 4, and 0% activation of total excitatory synapses. In subthreshold conditions, from *left to right* at level marked, curves represent measurements with 100, 64, 0, 32, 16, 8, and 4% activation of total excitatory synapses. Gray lines represent conditions under which the somatic membrane potential would exceed the threshold for repetitive activity in subthreshold conditions. *B*: percentage increase in equivalent level of uniform inhibition in suprathreshold conditions compared with subthreshold conditions. Results are shown for all 4 neurons. From *top to bottom* at level marked, curves represent measurements with 0, 4, 8, 16, 32, 64, and 100% activation of total excitatory synapses, except for RC4a where curves represent measurements with 4, 0, 8, 16, 32, 64, and 100% activation of total excitatory synapses. *x*-axis and *y*-axis of the graphs for RC1a, RC2a, and RC4a are the same as the *x*-axis and *y*-axis of the graph for RC4a, respectively. Gray lines represent conditions under which the somatic membrane potential would exceed the threshold for repetitive activity in subthreshold conditions.

produced by each activated excitatory synapse. To assess these changes, we calculated the derivative of I_N with respect to the number of inhibitory synapses activated (Fig. 4*A*, proximal inhibition: $dI_N/dsynapse_{i,prox}$; uniform inhibition: $dI_N/dsynapse_{i,uni}$) and the derivative of ΔV_m with respect to the number of inhibitory synapses activated (Fig. 4*B*, proximal inhibition: $d\Delta V_m/dsynapse_{i,prox}$; uniform inhibition: $d\Delta V_m/dsynapse_{i,uni}$) at various levels of synaptic excitation. These derivatives represent the instantaneous synaptic output at each level of synaptic inhibition. Greater magnitudes of these derivatives indicate a greater inhibition. The relative differences between $dI_N/dsynapse_{i,prox}$ and $dI_N/dsynapse_{i,uni}$ and between $d\Delta V_m/dsynapse_{i,prox}$ and $d\Delta V_m/dsynapse_{i,uni}$ provide a measure

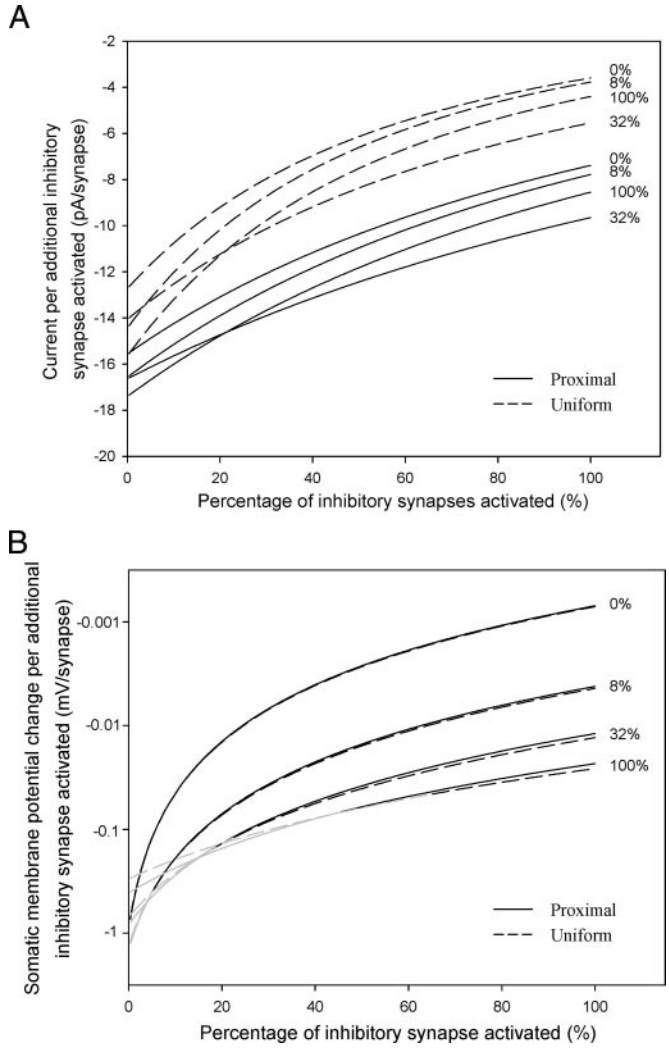

FIG. 4. Instantaneous synaptic output produced per each additional activated inhibitory synapse at varying levels of excitatory and inhibitory synaptic activity. *A*: current reaching the cell body produced by each additional activated inhibitory synapse. Solid lines represent simulations with proximal inhibition ($dI_N/dsynapse_{i,prox}$). Dashed black lines represent simulations with uniform inhibition ($dI_N/dsynapse_{i,uni}$). Numbers at the *right* of each pair of curves indicate the level of excitatory activity. *B*: somatic membrane potential change produced by each additional activated inhibitory synapse. Solid lines represent simulations with proximal inhibition ($d\Delta V_m/dsynapse_{i,prox}$). Dashed lines represent simulations with uniform inhibition ($d\Delta V_m/dsynapse_{i,uni}$). Numbers at the *right* of each pair of curves indicate the level of excitatory activity. Gray lines represent conditions under which the somatic membrane potential would exceed the threshold for repetitive activity in subthreshold conditions. *y*-axis is logarithmically scaled.

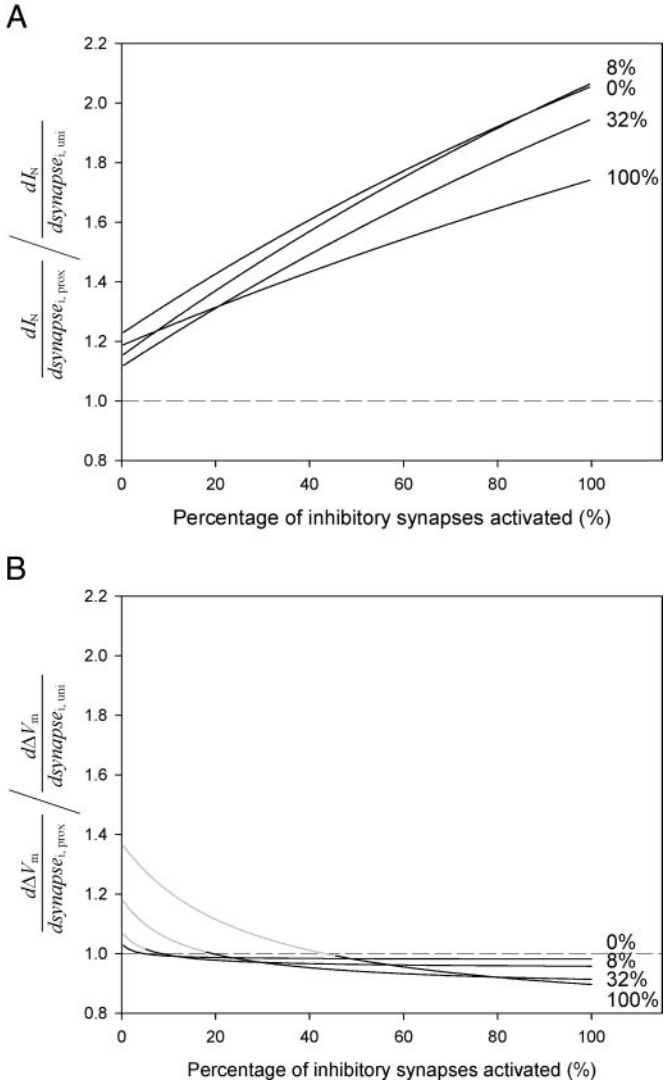

FIG. 5. Ratio of instantaneous synaptic output at varying levels of synaptic excitation and inhibition. Numbers at the *right* of each curve indicate the level of excitatory activity. *A*: ratio of $dI_N/dsynapse_{i,prox}$ over $dI_N/dsynapse_{i,uni}$. *B*: ratio of $d\Delta V_m/dsynapse_{i,prox}$ over $d\Delta V_m/dsynapse_{i,uni}$. Gray lines represent conditions under which the somatic membrane potential would exceed the threshold for repetitive activity in subthreshold conditions.

of the disparity in instantaneous inhibition produced by proximally and uniformly distributed inhibitory synapses. Note that the magnitude of $dI_N/dsynapse_{i,prox}$ is always greater than that of $dI_N/dsynapse_{i,uni}$ at comparable levels of excitation. The same is not true for the magnitude of $d\Delta V_m/dsynapse_{i,prox}$ compared to that of $d\Delta V_m/dsynapse_{i,uni}$.

To facilitate the comparison between proximal and uniform inhibition in the subthreshold and the suprathreshold regime, we calculated the ratio of $d\Delta V_m/dsynapse_{i,prox}$ to $d\Delta V_m/dsynapse_{i,uni}$ and the ratio of $dI_N/dsynapse_{i,prox}$ to $dI_N/dsynapse_{i,uni}$ (Fig. 5). These ratios provide a measure of the instantaneous difference in synaptic output at a particular level of synaptic activity. For each level of synaptic inhibition, values >1 indicate that the next synapse activated that is distributed under the proximal inhibition will be more effective than the next synapse activated that is distributed under the uniform inhibition. Proximal inhibition is instantaneously more effective in both the subthreshold and suprathreshold regime at low levels of inhibition

as indicated by the fact that for both ratios the values are >1. However, the decreasing ratio of $d\Delta V_m/dsynapse_{i,prox}$ to $d\Delta V_m/dsynapse_{i,uni}$ indicates that the comparative effectiveness of proximal inhibition over uniform inhibition in subthreshold conditions decreases with increasing inhibitory activity to the point where uniform inhibition becomes more effective than proximal inhibition (Fig. 5*B*). In contrast, proximal inhibition becomes increasingly more effective than uniform inhibition in the suprathreshold regime as indicated by the increasing ratio of $dI_N/dsynapse_{i,prox}$ to $dI_N/dsynapse_{i,uni}$ with increasing inhibitory activity (Fig. 5*A*).

DISCUSSION

By using compartmental models, we compared the inhibition produced by glycinergic/GABAergic inputs to Renshaw cells, which are distributed in a predominantly somatic and juxtasomatic manner (Alvarez et al. 1997), with the inhibition produced by the same number of inputs distributed with no regional bias. Our results show that, as expected, proximal inhibition is more effective in suppressing cell excitability than uniform inhibition in subthreshold conditions. Contrary to our expectations, the simulations showed that proximal inhibition was also more effective than uniform inhibition in suprathreshold conditions. Indeed the effectiveness of proximal inhibition relative to uniform inhibition was more marked under suprathreshold conditions than when observed under subthreshold conditions.

Mechanisms contributing to greater effectiveness of proximal inhibition over uniform inhibition in suprathreshold conditions

The instantaneous inhibition produced by both types of inhibition in subthreshold and in suprathreshold conditions, $d\Delta V_m/dsynapse_{i,prox}$, $d\Delta V_m/dsynapse_{i,uni}$, $dI_N/dsynapse_{i,prox}$, and $dI_N/dsynapse_{i,uni}$, provides insights into the biophysical mechanisms that lead to the greater effectiveness of proximal inhibition over uniform inhibition. In particular, the ratio of $d\Delta V_m/dsynapse_{i,prox}$ to $d\Delta V_m/dsynapse_{i,uni}$ reveals that with increasing levels of synaptic inhibition, each subsequently activated inhibitory synapse distributed proximally becomes less effective than if distributed uniformly in subthreshold conditions. In contrast, the ratio of $dI_N/dsynapse_{i,prox}$ to $dI_N/dsynapse_{i,uni}$ reveals that each subsequently activated inhibitory synapse distributed proximally becomes more effective than if distributed uniformly in suprathreshold conditions. These two opposing trends are attributed to the somatic quasi–voltage clamp produced by the repetitive firing of action potentials. By clamping the membrane potential of the soma and juxtasomatic regions of the dendritic tree, the quasi–voltage clamp has a greater stabilizing influence over the inhibitory driving potential of synapses distributed proximally than distributed uniformly. Thus as the activity of inhibitory synapses increases, synapses distributed proximally do not shunt each other and continue to generate the same level of hyperpolarizing current. In contrast, uniformly distributed synapses have a greater probability of shunting each other, thus decreasing their output. In the subthreshold regime, there is no somatic voltage clamp to prevent the mutual shunting of inhibitory inputs distributed proximally. In fact, as the level of synaptic excitation increases, the excitation acts to clamp the driving potential of the inhibitory inputs. Because the excitatory inputs to Renshaw cells are distributed with a distal bias, the clamping of the inhibitory driving potential will be greater for distal inputs than for proximal inputs. This is supported by the greater instantaneous effectiveness of uniformly distributed inhibitory inputs over that of proximally distributed inputs at higher levels of activity in the subthreshold regime.

Methodological considerations

SOMATIC VOLTAGE CLAMP IN SUPRATHRESHOLD CONDITIONS. The greater effectiveness of proximal inhibition over uniform inhibition is a product of the somatic voltage clamp in suprathreshold conditions. During the repetitive firing of action potentials, the soma is virtually clamped to the average membrane potential (Koch et al. 1995). This average value becomes less negative with increasing frequency of firing. In our models, we clamped the membrane potential to a single arbitrary value, −55 mV, to replicate suprathreshold conditions. If the somatic quasi–voltage clamp were to become less negative because of an increased frequency of firing, the current delivered by all inhibitory synapses would increase in magnitude. However, a gradient in the membrane potential with distance away from the cell body would still exist. The limited spatial extent of the voltage clamp would therefore lead to a greater clamping of the inhibitory driving potential for proximal inhibition than uniform inhibition. Thus our conclusion that proximal inhibition is even more effective than uniform inhibition in suprathreshold conditions compared with subthreshold conditions would still hold.

PASSIVE DENDRITES. To the best of our knowledge, the voltage-gated channels in the dendrites of Renshaw cells have not been described. Therefore we modeled their dendrites as passive. However, any source of active inward depolarizing currents located in the dendrites could increase the effectiveness of distally distributed inhibitory synapses through the deactivation of such currents.

MODELING OF SYNAPSES. The use of compartmental modeling provides a powerful means of directly comparing the effectiveness of different distributions of inhibitory synapses. Because all other factors are fixed, such as dendritic geometry and synaptic conductance, the effect of changes in synaptic distribution can be readily identified. However, the value of this strategy depends on the accuracy of the parameters assigned to the synapses.

Although gephyrin is predominantly linked with glycine receptor subunits (Schmitt et al. 1987), colocalization of gephyrin immunoreactive patches and $GABA_A$ subunits has been detected in Renshaw cells (Geiman et al. 2002). Approximately 70% of boutons to Renshaw cells display immunoreactivity to both glycine and GABA (Geiman et al. 2002). In our models, all inhibitory synapses were modeled as glycine/GABAergic. Although this might overestimate the strength of inhibition, the key results were independent of the strength of inhibition.

We are unaware of experimental observations regarding the time course of unitary coreleased glycine/GABA IPSPs to Renshaw cells. To model these inputs to Renshaw cells, relevant parameters were estimated using values reported for

glycine/GABA inputs to other spinal cord neurons (Jonas et al. 1998; Keller et al. 2001; Schneider and Fyffe 1992). The kinetics of cholinergic transmission to Renshaw cells has been studied by Dourado and Sargeant (2002). Parameters that could not be interpolated from their study were estimated from other studies of the $\alpha_4\beta_2$ ACh receptor (Buisson et al. 1996; Charnet et al. 1992; Covernton et al. 1994; Figl et al. 1998; Haghighi and Cooper 1998; Nelson and Lindstrom 1999; Sacchi et al. 1998). The conclusions based on our simulations were robust over a wide range of tonic excitatory and inhibitory synaptic activity. Thus any errors arising from overestimates and underestimates of the conductances associated with glycine/GABAergic and cholinergic synapses, as well as frequencies of activation, are unlikely to alter our conclusion that the effectiveness of proximal inhibition over uniform inhibition is greater in suprathreshold conditions.

Physiological implications

Our results provide evidence that distributing inhibitory synapses closer to the cell body produces more effective suppression of the excitability of a cell, particularly if the cell is already firing action potentials. In addition to Renshaw cells, there are other instances in the nervous system of proximally distributed inhibitory synapses. The majority of synapses found in the perisomatic region of cortical pyramidal cells are GABAergic (DeFelipe and Farinas 1992). Similarly, innervation of the perisomatic regions of pyramidal cells of the hippocampus is predominantly GABAergic (Megías et al. 2001). In both cases, the proximally distributed inhibitory inputs produce a stronger inhibition than distally distributed inhibition (Trevelyan and Watkinson 2005; Yang et al. 2003). Furthermore, a comparison of proximally and distally distributed inhibition in spiny neurons of the neostriatum also showed that proximal inhibition is more potent (Koos et al. 2004). It is likely that the effectiveness of proximal inhibition over more distal inhibition will be increased in suprathreshold conditions, compared with that in subthreshold conditions, for these cell classes as well.

The majority of Renshaw cell excitatory inputs come from α-motoneuron axon collaterals (Alvarez et al. 1999). In fact, Renshaw cells are very sensitive to motor axon activity (Hamm et al. 1987; Ross et al. 1976; Van Keulen 1979). In turn, Renshaw cells send inhibitory projections to α-motoneurons. It was initially thought that this connection produced a weak inhibition (Lindsay and Binder 1991; Maltenfort et al. 1998; Windhorst 1996). However, it has been recently demonstrated that in the presence of monoamines, Renshaw cell activation can deactivate the strong synaptic amplification of motoneurons mediated by persistent inward currents (Hultborn et al. 2003), thereby decreasing the excitability of motoneurons (Maltenfort et al. 2004). The robustness of the potent inhibitory control of Renshaw cells, resulting from the subcellular compartmentalization of their synaptic inhibitory inputs, may thus have important repercussions for the regulation of motoneuron excitability and, ultimately, motor control.

ACKNOWLEDGMENTS

We thank A. Pollett, S. Woods, and S. Cushing for assistance with the in-house computer software. We also thank G. Grande and K. Fenrich for helpful comments regarding the manuscript.

GRANTS

This work was supported in part by the National Institutes of Health. T. V. Bui was supported in part by a Natural Sciences and Engineering Research Council of Canada Postgraduate grant.

REFERENCES

Alvarez FJ, Dewey DE, Harrington DA, and Fyffe RE. Cell-type specific organization of glycine receptor clusters in the mammalian spinal cord. *J Comp Neurol* 379: 150–170, 1997.

Alvarez FJ, Dewey DE, McMillin P, and Fyffe RE. Distribution of cholinergic contacts on Renshaw cells in the rat spinal cord: a light microscopic study. *J Physiol* 515: 787–797, 1999.

Baldiserra F, Hultborn H, and Illert M. Integration in spinal neuronal systems. In: *Handbook of Physiology. The Nervous System. Motor Control*. Bethesda, MD: Am. Physiol. Soc., 1981, vol. II.

Barrett JN and Crill WE. Specific membrane properties of cat motoneurones. *J Physiol* 239: 301–324, 1974.

Bernander O, Douglas RJ, Martin KA, and Koch C. Synaptic background activity influences spatiotemporal integration in single pyramidal cells. *Proc Natl Acad Sci USA* 88: 11569–11573, 1991.

Brizzi L, Meunier C, Zytnicki D, Donnet M, Hansel D, D'Incamps BL, and Van Vreeswijk C. How shunting inhibition affects the discharge of lumbar motoneurones: a dynamic clamp study in anaesthetized cats. *J Physiol* 558: 671–683, 2004.

Bui TV, Cushing S, Dewey D, Fyffe RE, and Rose PK. Comparison of the morphological and electrotonic properties of Renshaw cells, Ia inhibitory interneurons, and motoneurons in the cat. *J Neurophysiol* 90: 2900–2918, 2003.

Buisson B, Gopalakrishnan M, Arneric SP, Sullivan JP, and Bertrand D. Human alpha4beta2 neuronal nicotinic acetylcholine receptor in HEK 293 cells: a patch-clamp study. *J Neurosci* 16: 7880–7891, 1996.

Carnevale NT, Woolf TB, and Shepherd GM. Neuron simulations with SABER. *J Neurosci Methods* 33: 135–148, 1990.

Charnet P, Labarca C, Cohen BN, Davidson N, Lester HA, and Pilar G. Pharmacological and kinetic properties of alpha 4 beta 2 neuronal nicotinic acetylcholine receptors expressed in Xenopus oocytes. *J Physiol* 450: 375–394, 1992.

Covernton PJ, Kojima H, Sivilotti LG, Gibb AJ, and Colquhoun D. Comparison of neuronal nicotinic receptors in rat sympathetic neurones with subunit pairs expressed in Xenopus oocytes. *J Physiol* 481: 27–34, 1994.

DeFelipe J and Farinas I. The pyramidal neuron of the cerebral cortex: morphological and chemical characteristics of the synaptic inputs. *Prog Neurobiol* 39: 563–607, 1992.

Dourado M and Sargent PB. Properties of nicotinic receptors underlying Renshaw cell excitation by alpha-motor neurons in neonatal rat spinal cord. *J Neurophysiol* 87: 3117–3125, 2002.

Eccles JC, Eccles DM, and Fatt P. Pharmacological investigations on a central synapse operated by acetylcholine. *J Physiol* 131: 154–169, 1956.

Eccles JC, Fatt P, and Koketsu K. Cholinergic and inhibitory synapses in a pathway from motor-axon collaterals to motoneurones. *J Physiol* 126: 524–562, 1954.

Figl A, Viseshakul N, Shafaee N, Forsayeth J, and Cohen BN. Two mutations linked to nocturnal frontal lobe epilepsy cause use-dependent potentiation of the nicotinic ACh response. *J Physiol* 513: 655–670, 1998.

Gabbiani F, Midtgaard J, and Knopfel T. Synaptic integration in a model of cerebellar granule cells. *J Neurophysiol* 72: 999–1009, 1994.

Geiman EJ, Zheng W, Fritschy JM, and Alvarez FJ. Glycine and GABA(A) receptor subunits on Renshaw cells: relationship with presynaptic neurotransmitters and postsynaptic gephyrin clusters. *J Comp Neurol* 444: 275–289, 2002.

Gonzàlez-Forero D, Pastor AM, Geiman EJ, Benitez-Temino B, and Alvarez FJ. Regulation of gephyrin cluster size and inhibitory synaptic currents on Renshaw cells by motor axon excitatory inputs. *J Neurosci* 25: 417–429, 2005.

Haghighi AP and Cooper E. Neuronal nicotinic acetylcholine receptors are blocked by intracellular spermine in a voltage-dependent manner. *J Neurosci* 18: 4050–4062, 1998.

Hamm TM, Sasaki S, Stuart DG, Windhorst U, and Yuan CS. The measurement of single motor-axon recurrent inhibitory post-synaptic potentials in the cat. *J Physiol* 388: 631–651, 1987.

Heckman CJ and Binder MD. Analysis of effective synaptic currents generated by homonymous Ia afferent fibers in motoneurons of the cat. *J Neurophysiol* 60: 1946–1966, 1988.

Hille B. *Ion Channels of Excitable Membranes.* Sunderland, MA: Sinauer, 2001.

Holt GR and Koch C. Shunting inhibition does not have a divisive effect on firing rates. *Neural Comput* 9: 1001–1013, 1997.

Hultborn H, Denton ME, Wienecke J, and Nielsen JB. Variable amplification of synaptic input to cat spinal motoneurones by dendritic persistent inward current. *J Physiol* 552: 945–952, 2003.

Hultborn H and Pierrot-Deseilligny E. Input–output relations in the pathway of recurrent inhibition to motoneurones in the cat. *J Physiol* 297: 267–287, 1979.

Jonas P, Bischofberger J, and Sandkuhler J. Corelease of two fast neurotransmitters at a central synapse. *Science* 281: 419–424, 1998.

Katz R and Pierrot-Deseilligny E. Recurrent inhibition in humans. *Prog Neurobiol* 57: 325–355, 1999.

Keller AF, Coull JA, Chery N, Poisbeau P, and De Koninck Y. Region-specific developmental specialization of GABA-glycine cosynapses in laminas I–II of the rat spinal dorsal horn. *J Neurosci* 21: 7871–7880, 2001.

Koch C. *Biophysics of Computation: Information Processing in Single Neurons.* New York: Oxford Univ. Press, 1999.

Koch C, Bernander O, and Douglas RJ. Do neurons have a voltage or a current threshold for action potential initiation? *J Comput Neurosci* 2: 63–82, 1995.

Koch C, Poggio T, and Torre V. Nonlinear interactions in a dendritic tree: localization, timing, and role in information processing. *Proc Natl Acad Sci USA* 80: 2799–2802, 1983.

Koos T, Tepper JM, and Wilson CJ. Comparison of IPSCs evoked by spiny and fast-spiking neurons in the neostriatum. *J Neurosci* 24: 7916–7922, 2004.

Lagerback PA. An ultrastructural study of serially sectioned Renshaw cells. III. Quantitative distribution of synaptic boutons. *Brain Res* 264: 215–223, 1983.

Lee RH and Heckman CJ. Adjustable amplification of synaptic input in the dendrites of spinal motoneurons in vivo. *J Neurosci* 20: 6734–6740, 2000.

Lindsay AD and Binder MD. Distribution of effective synaptic currents underlying recurrent inhibition in cat triceps surae motoneurons. *J Neurophysiol* 65: 168–177, 1991.

Maltenfort MG, Heckman CJ, and Rymer WZ. Decorrelating actions of Renshaw interneurons on the firing of spinal motoneurons within a motor nucleus: a simulation study. *J Neurophysiol* 80: 309–323, 1998.

Maltenfort MG, McCurdy ML, Phillips CA, Turkin VV, and Hamm TM. Location and magnitude of conductance changes produced by Renshaw recurrent inhibition in spinal motoneurons. *J Neurophysiol* 92: 1417–1432, 2004.

Megias M, Emri Z, Freund TF, and Gulyas AI. Total number and distribution of inhibitory and excitatory synapses on hippocampal CA1 pyramidal cells. *Neuroscience* 102: 527–540, 2001.

Nelson ME and Lindstrom J. Single channel properties of human alpha3 AChRs: impact of beta2, beta4 and alpha5 subunits. *J Physiol* 516: 657–678, 1999.

Oleskevich S, Alvarez FJ, and Walmsley B. Glycinergic miniature synaptic currents and receptor cluster sizes differ between spinal cord interneurons. *J Neurophysiol* 82: 312–319, 1999.

Powers RK and Binder MD. Summation of effective synaptic currents and firing rate modulation in cat spinal motoneurons. *J Neurophysiol* 83: 483–500, 2000.

Rall W. Core conductor theory and cable properties of neurons. In: *Handbook of Physiology. The Nervous System. Cellular Biology of Neurons*. Bethesda, MD: Am. Physiol. Soc., 1977, vol. 1, pt. 1.

Renshaw B. Central effects of centripetal impulses in axons of spinal ventral roots. *J Neurophysiol* 9: 191–204, 1946.

Ross HG, Cleveland S, and Haase J. Quantitative relation between discharge frequencies of a Renshaw cell and an intracellularly depolarized motoneuron. *Neurosci Lett* 3: 129–132, 1976.

Ryall RW. Renshaw cell mediated inhibition of Renshaw cells: patterns of excitation and inhibition from impulses in motor axon collaterals. *J Neurophysiol* 33: 257–270, 1970.

Sacchi O, Rossi ML, Canella R, and Fesce R. Synaptic current at the rat ganglionic synapse and its interactions with the neuronal voltage-dependent currents. *J Neurophysiol* 79: 727–742, 1998.

Schmitt B, Knaus P, Becker CM, and Betz H. The Mr 93,000 polypeptide of the postsynaptic glycine receptor is a peripheral protein. *Biochemistry* 26: 805–811, 1987.

Schneider SP and Fyffe RE. Involvement of GABA and glycine in recurrent inhibition of spinal motoneurons. *J Neurophysiol* 68: 397–406, 1992.

Stuart GJ and Redman SJ. Voltage dependence of Ia reciprocal inhibitory currents in cat spinal motoneurones. *J Physiol* 420: 111–125, 1990.

Trevelyan AJ and Watkinson O. Does inhibition balance excitation in neocortex? *Prog Biophys Mol Biol* 87: 109–143, 2005.

Ulrich D. Differential arithmetic of shunting inhibition for voltage and spike rate in neocortical pyramidal cells. *Eur J Neurosci* 18: 2159–2165, 2003.

Van Keulen L. Autogenetic recurrent inhibition of individual spinal motoneurones of the cat. *Neurosci Lett* 21: 297–300, 1981.

Walmsley B and Tracey DJ. An intracellular study of Renshaw cells. *Brain Res* 223: 170–175, 1981.

Windhorst U. On the role of recurrent inhibitory feedback in motor control. *Prog Neurobiol* 49: 517–587, 1996.

Yang KH, Franaszczuk PJ, and Bergey GK. The influences of somatic and dendritic inhibition on bursting patterns in a neuronal circuit model. *Biol Cybern* 89: 242–253, 2003.